THE X-RAY JET IN CENTAURUS A: CLUES TO THE JET STRUCTURE AND PARTICLE ACCELERATION

Jun Kataoka,[1] Łukasz Stawarz,[2,3] Felix Aharonian,[2] Fumio Takahara,[4]
Michał Ostrowski,[3] and Philip G. Edwards[5]

ABSTRACT

We report detailed studies of the X-ray emission from the kiloparsec-scale jet in the nearest active galaxy, Centaurus A. By analyzing the highest quality X-ray data obtained with the *Chandra* ACIS-S, 41 compact sources (mostly bright jet knots) were found within the jet on angular scales less than $4''$, 13 of which were newly identified. We construct the luminosity function for the detected jet knots and argue that the remaining emission is most likely to be truly diffuse, rather than resulting from the sum of many unresolved fainter knots. We subtracted the contributions of the bright knots from the total X-ray jet flux, and show that the remaining extended emission has a relatively flat-topped intensity profile in the transverse jet direction, with the intensity peaking at the jet boundaries between $50''$ and $170''$. We note that limb-brightened morphologies have been observed previously at radio frequencies in a few FR I and FR II jet sources, but never so clearly at higher photon energies. Our result therefore supports a stratified jet model, consisting of a relativistic outflow including a boundary layer with a velocity shear. In addition, we found that the X-ray spectrum of the diffuse component is almost uniform across and along the jet, with an X-ray energy spectral index of $\alpha_X \approx 1$, similar to those observed in the compact knots. We discuss this spectral behavior within a framework of shock and stochastic particle acceleration processes, connected with the turbulent, supersonic, and nonsteady nature of the relativistic outflow. We note some evidence for a possible spectral hardening at the outer sheath of the jet, and manifesting itself in observed X-ray spectra of $\alpha_X < 0.5$ in the most extreme cases. Due to the limited photon statistics of the present data, further deep observations of Centaurus A are required to determine the reality of this finding; however, we note that the existence of the hard X-ray features at outer jet boundaries would provide an important challenge to theories for the evolution of ultrarelativistic particles within extragalactic jets.

Subject headings: acceleration of particles — galaxies: individual (Centaurus A) — galaxies: jets —
radiation mechanisms: nonthermal — X-rays: general

1. INTRODUCTION

The *Chandra X-Ray Observatory* has confirmed that X-ray emission from large-scale jets is common in radio galaxies and quasars (e.g., Harris & Krawczynski 2002; Kataoka & Stawarz 2005 and references therein). In nearby FR I sources, the typical radio to X-ray spectrum of kiloparsec-scale jet knots is consistent with a single, smoothly broken power-law continuum, suggesting that this broadband emission is entirely due to nonthermal synchrotron radiation from a single electron population (e.g., Hardcastle et al. 2001 for 3C 66B), although spatial offsets observed in these sources between the positions of the X-ray and radio knots may indicate a more complicated physical picture. Meanwhile, the observed X-ray knots in 100 kpc scale quasar jets are much brighter than expected from a simple extrapolation of the radio-to-optical fluxes (e.g., Schwartz et al. 2000 for PKS 0637–752). This has led to the hypothesis that the X-ray production involved inverse Comptonization of cosmic microwave background photons within a highly relativistic flow (Tavecchio et al. 2000; Celotti et al. 2001). It has been argued, however, based on recent studies of multiwavelength properties of powerful large-

scale jets, that the inverse Compton model may face serious problems (see, e.g., the discussion in Stawarz et al. 2004; Kataoka & Stawarz 2005). Moreover, the inverse Compton model cannot readily explain the detected X-ray emission from a few FR II jets—Pictor A (Wilson et al. 2001), 3C 303 (Kataoka et al. 2003), 3C 120 (Harris et al. 2004), and 3C 403 (Kraft et al. 2005)—since they are expected to be the *debeamed* analogs of the radio-loud quasars. Therefore, the synchrotron origin of the keV photons remains a plausible alternative even for powerful FR II/quasar jets.

The synchrotron model for X-ray emission from the large-scale jets in radio galaxies (FR I/FR II) and quasars involves much lower bulk velocities for the flows, but on the other hand, it requires the presence of ultrarelativistic electrons with energies $E_e \geq 100$ TeV. This requirement is supported in a natural way by the expectation that the large-scale jets are good candidates for the the acceleration of cosmic-ray particles owing to their large, extended structures and turbulent nature (see Hillas 1984). From the theoretical perspective, it has been proposed that the most energetic particles are accelerated preferentially in the turbulent boundary layers of such outflows (Ostrowski 2000; Stawarz & Ostrowski 2002; see also in this context Rieger & Duffy 2004 and references therein). In fact, the "limb-brightened" jet morphology expected in this type of models has been observed at radio frequencies (probing relatively low electron energies) in several objects, such as M87 (FR I; Owen et al. 1989) and 3C 353 (FR II; Swain et al. 1998). More importantly, the continuous acceleration processes acting thereby should result in the formation of flat spectra at the highest electron energies, which may account for the hard X-ray spectra and high X-ray luminosities of powerful jet sources. Similarly, Dermer & Atoyan (2002)

[1] Tokyo Institute of Technology, 2-12-1, Meguro-ku, Ohokayama, Tokyo 152-8551, Japan; kataoka@hp.phys.titech.ac.jp.

[2] Max-Planck-Institut für Kernphysik, Heidelberg, Germany; lukasz.stawarz@mpi-hd.mpg.de, felix.aharonian@mpi-hd.mpg.de.

[3] Obserwatorium Astronomiczne, Uniwersytet Jagielloński, Kraków; Poland; mio@oa.uj.edu.pl.

[4] Osaka University, Toyonaka, Osaka, Japan; takahara@vega.ess.sci.osaka-u.ac.jp.

[5] Institute of Space and Astronautical Science, JAXA, Sagamihara, Japan; pge@vsop.isas.jaxa.jp.

suggested the formation of high-energy spectral hardening owing to inefficient Klein-Nishina radiative losses of electrons, which also could appear at X-ray energies for some particular choices of jet parameters. Therefore, the investigations of (1) the transverse structure of X-ray jets, and (2) the spectral properties of diffuse X-ray jet emission, provide important clues for an understanding of the production of cosmic-ray particles and the origin of hard X-ray emission in large-scale jets. Unfortunately, only few such studies have been reported so far, mainly due to the technical difficulties. In fact, it is generally impossible to resolve jets in low power FR I radio galaxies or distant quasars, even with the excellent spatial resolution (0″.5 half-power diameter on-axis) and sensitivity of *Chandra*.[6]

Centaurus A (hereafter Cen A) is the nearest active galaxy ($d = 3.4$ Mpc, for which $1''$ corresponds to 16 pc) and has been well studied across the entire electromagnetic spectrum at the highest linear spatial resolution (Israel 1998). It is considered to be a prototypical FR I radio galaxy, although the one-sidedness of its kiloparsec-scale jet and the presence of the outer, megaparsec-scale radio lobes is unusual for this type of object. Previous observations of Cen A have resulted in the detection of a bright X-ray and radio jet extending $\geq 4'$ northeast of the nucleus (Schreier et al. 1979; 1981; Clarke et al. 1986, 1992; Kraft et al. 2002; Hardcastle et al. 2003). From the analysis of the broadband radio to X-ray jet emission, the synchrotron origin of keV photons has been established for the bright knots, which are characterized by a minimum pressure $\sim 10^{-9}$ dyn cm^{-2}, equipartition magnetic field $\sim 100~\mu$G and $1-10$ keV luminosities of the order of $\sim 10^{39}$ ergs s^{-1}. In addition, a very complex morphology of the whole outflow was noted in both the radio and X-ray bands, including the presence of bright filaments and diffuse extended regions with complex substructure. The diffuse X-ray emission clearly extends to the edge of the radio jet and is reasonably well matched to the radio emission on these scales. Moreover, Hardcastle et al. (2003) noted two conspicuous regions where the extended X-ray emission appeared to be associated with the edges of the jet, and to be absent in the center. These X-ray edges of the jet have no obvious radio counterparts, although Clarke et al. (1986, 1992) also reported a limbbrightened radio morphology in some sections of the jet. We note that these radio polarization studies indicated a projected magnetic field parallel to the jet axis along the whole jet length.

Stimulated by these previous reports, the goal of this work is twofold, namely, determining the transverse profile of the diffuse X-ray emission extending over the Cen A jet and constraining its spectral properties. Our approach differs from previous studies in that we focus on the diffuse emission rather than the bright jet knots, which are thought to be compact shocks inside the jet (Hardcastle et al. 2003). We remove the contributions from the knots, as particle acceleration may take place in quite different manners in different jet regions (but we revisit this problem later in the discussion section). The paper is organized as follows. In § 2 we describe the *Chandra* observations, data reduction process, and our analysis method. In § 3 we present the results of the data analysis. In § 4 we discuss our findings in the context of particle acceleration models, presenting our conclusions in § 5.

2. DATA REDUCTION

Since the launch of *Chandra X-Ray Observatory* in 1999 July, X-ray observations of Cen A have been conducted 10 times, three of which were for calibration (CAL) purposes, and the

remaining for General Observer (GO) or Guaranteed Time Observing (GTO) proposals. The first *Chandra* X-ray image of Cen A was obtained with the microchannel plate X-ray imaging detector HRC-I (ObsIDs 463, 1253, and 1412), and the results were presented in Kraft et al. (2000). The first useful spectral information was subsequently presented based on observations using the ACIS-I configuration (ObsIDs 316 and 962; Kraft et al. 2002). The exposure times for the two observations were 35.9 and 36.5 ks, respectively. Although the jet was $4'-5'$ off-axis from the aim point in these observations, and the image resolution was therefore significantly degraded, 31 knots in the Cen A jet were successfully detected.

More recent *Chandra* observations of Cen A were made in 2002 September (ObsID 2978) and 2003 September (ObsID 3965) using the standard ACIS-S configuration, where the back-illuminated S3 chip was focused to obtain maximal sensitivity to soft photons. The exposure times for the two observations were 45.2 and 50.2 ks, respectively. The active nucleus was at the aim point, resulting in both subarcsecond resolution and good spectral sensitivity for the whole inner part of the jet in Cen A. Although the imaging degrades substantially for sources more than $1'$ off-axis, and the X-ray jet in Cen A extends over $\sim 4'$ in length, the encircled energy for a point source is contained within a diameter of $\sim 3''$ all along the outflow. The roll angle of the satellite was carefully chosen to avoid the readout streak of the bright nucleus impinging on the jet image. The results from the first observation, ObsID 2978, are given in Hardcastle et al. (2003). The X-ray image was compared with new, high dynamic range VLA images for one-to-one identification of radio knots, for which apparent subluminal motions were found (on scales of hundreds of parsecs). Here we analyze the combined ACIS-S data (ObsIDs 2978 and 3965) to obtain the best image resolution and spectral information reported to date.

A co-added, exposure-corrected image of the Cen A jet in the $0.4-8$ keV bandpass is shown in Figure 1 (*left*). The image is smoothed with a $\sigma = 0''.5$ Gaussian function. The nucleus is located in the southwest corner of the image, and the jet extends to the northeast. The figure shows that the diffuse emission from the jet is observed up to $\sim 4'$ from the nucleus. Also, the *Chandra* image shows that the X-ray jet consists of many knots of enhanced emission embedded within the diffuse regions, as described in detail by Kraft et al. (2002) and Hardcastle et al. (2003). Since the primary purpose of this paper is to study the characteristics of the *diffuse* X-ray emission associated with the jet, our approach is complementary to previous reports in the literature: we first resolve the pointlike sources within the jet (in projection).[7] Next we subtract the contributions from these point sources to enable a quantitative measurement of the diffuse X-ray emission. One may ask whether the remaining emission is truly diffuse in nature, or whether it is the summation of numerous unresolved jet knots at even smaller spatial scales. We revisit this problem in § 3.3, based on the luminosity function of the jet knots.

Using a wavelet decomposition source-detection algorithm (`wavdetect`; Vikhlinin et al. 1995) to detect emission enhancements on angular scales of 0″.5 and 1″, we find a total of 35 distinct knots or enhancements of X-ray emission embedded within the diffuse regions. We then extend the angular scales to 2″ and

---

[6] See *Proposers' Observatory Guide*, volume 7, at http://cxc.harvard.edu/proposer/POG/index.html.

[7] From a comparison of the source density within the jet and that in surrounding regions, it is highly likely that most of sources are jet knots, with only a few likely to be background, or foreground, sources (mainly X-ray binaries in Cen A). A check of the NASA/IPAC Extragalactic Database (NED) yielded only one possible identification, with an X-ray star. Similarly the chance probability that one of the new X-ray point sources discussed here is a background AGN is less than 1% (Kraft et al. 2001). See Table 1 for more details.
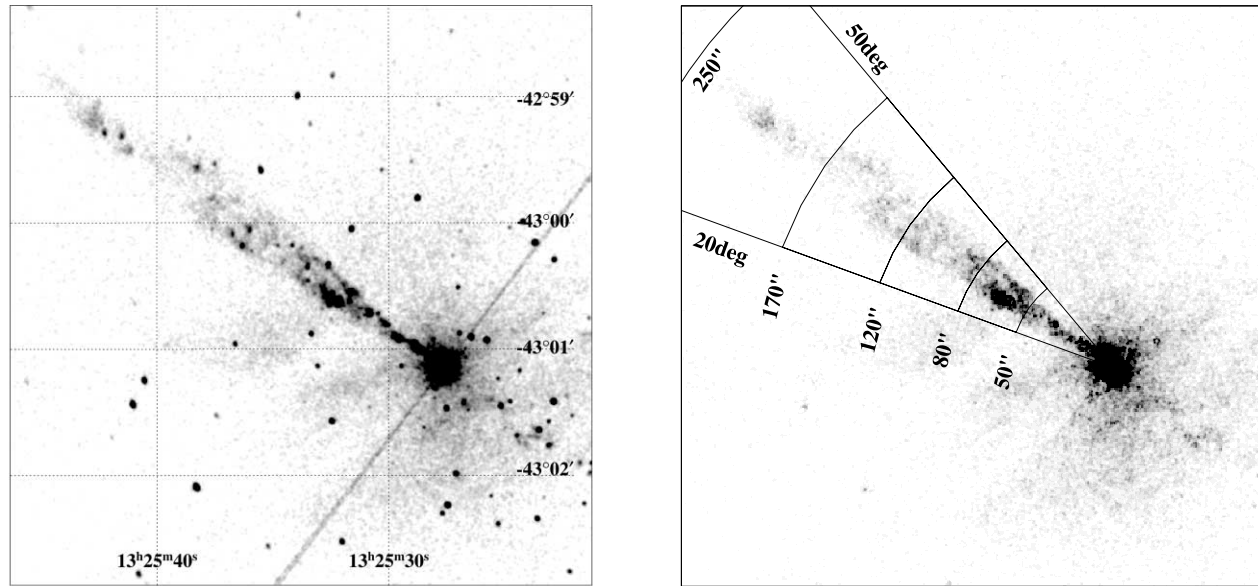
Fig. 1.—*Left:* 0.4–8.0 keV X-ray image of the Cen A jet. Archival data from ObsIDs 2978 and 3965 are combined. The image is smoothed with a $\sigma = 0\rlap{.}''5$ Gaussian. *Right:* 0.4–8.0 keV X-ray image of the Cen A jet, after subtracting the point sources and filling in the blanks with values interpolated from surrounding background regions. More details are given in the text. Definitions of the angle Θ and radial distance r are given in the panel.

$4''$, but only an additional six sources are found in these larger region sizes. This suggests that most of the jet knots in Cen A are very compact and that their extent is smaller than, or comparable to, that expected from the *Chandra* point-spread function (PSF). Our result is therefore consistent with findings by Kraft et al. (2000) and Hardcastle et al. (2003), who claimed that most of the X-ray knots are diffuse but at the $1''$ (~ 10 pc) level. Due to the good photon statistics and excellent angular resolution during the observations, the total number of the detected sources is significantly larger than that reported in the literature (i.e., 41 compared with 31 for Kraft et al. 2002). Three of the weaker knots reported in Kraft et al. (2002), NX1 (knot 1), EX3 (knot 19), and FX4 (knot 23), were not detected at the previous level in our high resolution, co-added ACIS-S image. The location, distance, and position angle of the 13 knots or enhancements that were newly detected in our analysis are listed in Table 1.

We next apply `dmfilth` implemented in the CIAO 3.2 package to replace the pixel values for the point sources detected by `wavdetect` with values interpolated from surrounding background regions (DIST option in `dmfilth`).[8] Here the source regions are defined as the ellipses output from `wavdetect` that contain at least a $3\,\sigma$ excess of photon counts over the background. The background is taken from the "donut-shaped" region surrounding the source, with the dimensions of the major and minor axes of the outer ellipse both doubled. The resultant image is almost flat, as expected, but contains a few irregular pixels with outstanding photon counts. This is because, in some regions, source ellipses overlap. The background region for a certain point source therefore inevitably contains photons from neighboring source regions. We therefore repeat the same process (i.e., source detection by `wavdetect` and smoothing by `dmfilth`) three times, until no irregular bins appeared in the image. The resultant X-ray image of the diffuse emission is given in Figure 1 (*right*; 0.4–8.0 keV). We also made bandpass images

[8] See *Science Threads for CIAO 3.2* at http://cxc.harvard.edu/ciao/threads/index.html.

TABLE 1
Newly Detected X-Ray Knots and Enhancements in the Cen A Jet

Knot ID	Distance (arcsec)	Angle (deg)	R.A. (J2000.0)	Decl. (J2000.0)	Net Counts
1..............	9.96	36.65	13 25 28.32	−43 01 02.8	159 ± 18
2..............	15.31	35.23	13 25 28.73	−43 00 59.9	$2682 \pm 55^{\mathrm{a}}$
3..............	35.56	36.96	13 25 30.16	−43 00 47.6	$244 \pm 17^{\mathrm{b}}$
4..............	40.96	39.41	13 25 30.45	−43 00 43.1	100 ± 12
5..............	55.65	35.06	13 25 31.69	−43 00 37.2	204 ± 19
6..............	65.96	31.96	13 25 32.63	−43 00 34.3	123 ± 13
7..............	80.78	40.48	13 25 33.12	−43 00 17.0	42 ± 8
8..............	89.48	40.05	13 25 33.75	−43 00 12.0	51 ± 10
9..............	86.64	37.35	13 25 33.79	−43 00 16.9	53 ± 10
10.............	82.92	32.40	13 25 33.89	−43 00 24.9	44 ± 9
11.............	107.94	31.10	13 25 35.90	−43 00 13.8	46 ± 9
12.............	163.57	38.42	13 25 39.10	−42 59 28.6	16 ± 5
13.............	209.89	37.59	13 25 42.52	−42 59 02.6	38 ± 8

Notes.—Thirteen new X-ray jet knots and enhancements have been detected, in addition to those in Table 2 of Kraft et al. (2002), in the co-added, 0.4–8.0 keV ACIS-S image. However, three knots in Kraft et al. (2002), namely, NX1 (knot 1), EX3 (knot 19), and FX4 (knot 23), were not detected at their previously reported levels for various reasons. NX1 is only $\leq 3''$ apart from the nucleus and can hardly be detected in our 0.4–8.0 keV bandpass due to strong contamination of the bright nucleus emission. Kraft et al. (2002) claimed a detection of NX1 using only the 0.4–1.5 keV bandpass image, since the heavily absorbed nucleus is expected to be suppressed. This is also the case in our analysis, but we adopted a more conservative approach. We find no evidence for any enhancement in the jet emission around EX3, suggesting that it may have been a statistical fluctuation. Finally, we suggest that FX4 is identical to FX3 reported in Kraft et al. (2002), but was regarded as a separate jet knot due to poor photon statistics. Units of right ascension are hours, minutes, and seconds, and units of declination are degrees, arcminutes, and arcseconds.

[a] This extremely bright knot is only $\sim 1\rlap{.}''5$ from the neighboring bright knot (R.A. $= 13^{\mathrm{h}}25^{\mathrm{m}}28\rlap{.}^{\mathrm{s}}57$, decl. $= -43'01''00\rlap{.}''1$) and therefore previously could not be resolved from AX1 or knot 2 in Table 2 of Kraft et al. 2003.

[b] This jet-knot may be identified with the X-ray star J132530.1−430048 reported in Colbert et al. (2004).
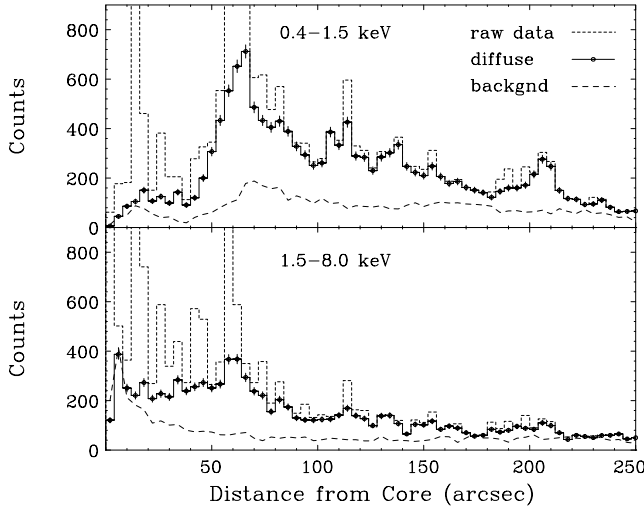
FIG. 2.—Longitudinal jet profile of the Cen A in the soft X-ray energy band (0.4–1.5 keV; *top*) and the hard X-ray energy band (1.5–8.0 keV; *bottom*), where the photons counts are integrated over the position angles $25° \leq \Theta \leq 45°$. The dotted histogram shows the profile derived from the raw X-ray image (Fig. 1, *left*), whereas the solid histogram with data points shows the one obtained for the diffuse emission only (Fig. 1, *right*). The dashed line shows the background profile compiled from $15° \leq \Theta \leq 25°$ and $45° \leq \Theta \leq 55°$ regions.

FIG. 3.—*Top:* The observed longitudinal X-ray intensity profile of the diffuse jet component in the 0.4–8.0 keV photon energy band. Photon counts are integrated over the position angle ranges $25° \leq \Theta \leq 45°$ (*histogram*), $25° \leq \Theta \leq 33°$ (*solid line*), $33° \leq \Theta \leq 37°$ (*dashed line*), and $37° \leq \Theta \leq 45°$ (*cross-hatched area*). *Bottom:* Variation of the hardness ratio along the main jet axis. Hardness is defined as the ratio between the X-ray counts measured in the soft X-ray energy band (0.4–1.5 keV) and the hard X-ray energy band (1.5–8.0 keV). Note that the hardness ratio changes significantly at the distance $r_c \simeq 50''$, but stays almost constant at larger distances. The dotted line shows the hardness changes for the background compiled from $15° \leq \Theta \leq 25°$ and $45° \leq \Theta \leq 55°$ regions.

for soft X-rays (0.4–1.5 keV) and hard X-rays (1.5–8.0 keV) using the same procedure.

3. DATA ANALYSIS AND RESULTS

In order to derive the intensity (photon counts) profile of the jet both in the longitudinal and transverse directions, we first define the position angle (Θ) and the distance (r) with respect to the nucleus of Cen A, as shown in Figure 1 (*right*). Note that the position angle is measured from east through north (i.e., in a clockwise direction in the figure). Then we can integrate the photon counts in a sector of an arbitrary range of r and Θ, to construct the intensity profile parallel or perpendicular to the jet main axis, which is given by $\Theta \sim 35°$. Since our approach is simply to sum the counts in each sector bounded by the stated values of r and θ, and not to derive the emissivity, no normalization by the area of each sector ($\propto 1/r^2$) was performed.

3.1. *Longitudinal Jet Profiles*

We first integrate the photon counts in each thin shell within a radial distance $r \sim r + \Delta r$ over the range of position angle $25° \leq \Theta \leq 45°$, and then construct the longitudinal intensity profile in $\Delta r = 4''$ steps, from $r = 0''$ to $r = 250''$. Figure 2 shows the longitudinal jet profiles thus produced, for both soft X-rays (0.4–1.5 keV; *top*) and hard X-rays (1.5–8.0 keV; *bottom*). The dotted histograms show the profiles derived from the raw X-ray images, whereas those for the diffuse X-ray emission are given as the data points on the solid-line histogram. We also show the intensity profile of the background (i.e., off-jet) region as a dashed line for comparison, where the background was accumulated in the $15° \leq \Theta \leq 25°$ and $45° \leq \Theta \leq 55°$ regions. The intensity profiles along the jet are quite different in the two energy bands, especially at the innermost part of the jet ($0'' \leq r \leq 50''$), where the soft X-ray photons are significantly absorbed in the dust lane crossing the Cen A host galaxy.

To see this more clearly, we divided the 1.5–8.0 keV longitudinal jet profile by that of the 0.4–1.5 keV, to check for hardness variations along the X-ray jet. Figure 3 compares the hardness ratio (HR) and the 0.4–8.0 keV X-ray intensity profile. One can
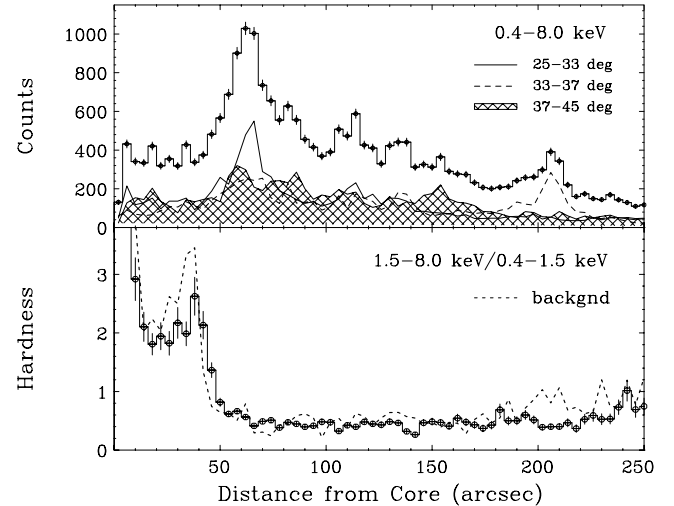
clearly see that HR changes significantly at $r_c \simeq 50''$, corresponding to a linear scale of ~ 800 pc. Obviously, such a dramatic change of the HR is not due to the changes of intrinsic jet spectrum. In fact, we can see that the HR changes in a similar way for the background region also, as shown by the dashed line in the bottom panel. The inner 1 kpc of the jet is observed through the dust lane of the galaxy, making detection of any optical component difficult (Israel 1998). This same dust lane, or equatorial gas, heavily absorbs soft X-rays as well, resulting in the significant changes of the hardness ratio seen in Figure 3. In the outer part of the jet ($50'' \leq r \leq 240''$), the HR is almost constant. This trend suggests that the X-ray spectrum does not change significantly along the jet, but the contribution from the background photons must be carefully examined before reaching this conclusion.

To find possible spectral changes along the jet, we fit the diffuse emission with a power-law function in XSPEC, for each shell in $\Delta r = 10''$ steps between $10''$ and $100''$, and $20''$ steps between $100''$ and $240''$. We do not examine the innermost part of the jet ($r \leq 10''$) because the X-ray emission from the nucleus significantly contaminates the jet emission there.[9] We take the background from neighboring shells just outside the jet ($15° \leq \Theta \leq 25°$, $45° \leq \Theta \leq 55°$ at the same range of r) and subtract it from the source spectrum. The result of spectral fitting along the jet is shown in Figure 4. As expected from the hardness profile, the X-ray spectrum clearly changes at a characteristic distance of $r_c \simeq 50''$. In the inner jet region ($r \leq r_c$), the spectrum is well represented by a power-law function heavily absorbed with a free zero-redshift absorbing column. A combined spectrum between $r = 10''$ and $50''$ gives the best-fit absorbing column

---

[9] The contamination level is quite uncertain, as the bright nucleus emission is strongly piled up. We, however, make a crude estimate that more than 80% of the photons come from the nucleus, rather than from the jet, within the most inner part ($r \leq 10''$) of the jet. See Fig. 2 for a comparison of background profile with the diffuse jet emission profile.
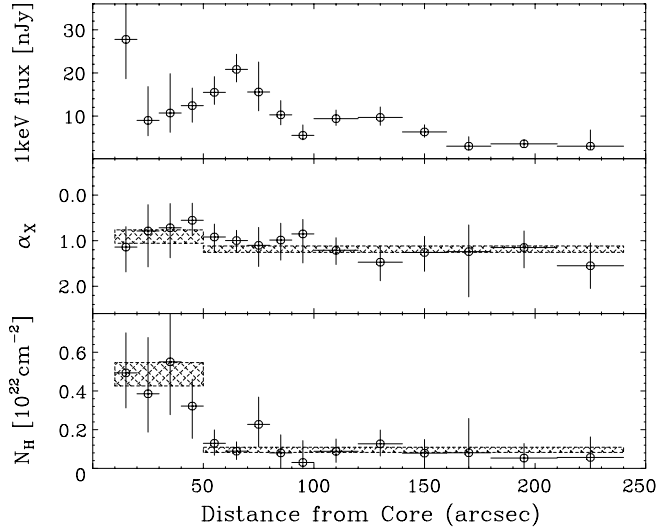
FIG. 4.—Variation of the X-ray flux density measured at 1 keV (*top*), the X-ray energy spectral index α_X (*middle*), and the absorbing column density N_H (*bottom*) of the diffuse emission along the jet. Note that N_H changes significantly at $r_c \simeq 50''$, but that the energy spectral index is almost constant ($\alpha_X \simeq 1$) along the jet. Hatched regions show the best-fit parameters and their 1 σ uncertainties for the combined spectral fittings within $10'' \leq r \leq 50''$ and $50'' \leq r \leq 250''$, respectively.

density of $N_H = (4.79^{+0.68}_{-0.53}) \times 10^{21}$ cm^{-2} and an intrinsic energy spectral index of $\alpha_X = 0.89^{+0.17}_{-0.13}$, where the reduced χ^2 is 0.50 for 164° of freedom (dof).

The absorption column in the outer region ($r \geq r_c$) is much smaller, and similar to the Galactic column density ($\sim 0.7 \times 10^{21}$ cm^{-2}). Although there is a weak trend of spectral steepening at larger distances from the nucleus, there is no sudden change in the spectral form over the wide distance of $r = 50''$ and $240''$. The subtle anticorrelation between the fitted X-ray spectral index and the X-ray flux which can be seen in Figure 4 is most likely due to minor variation of the fitted absorbing column density at $r \geq r_c$. The best-fit parameters for the average spectrum in this outer jet region are $N_H = (0.96 \pm 0.13) \times 10^{21}$ cm^{-2} and $\alpha_X = 1.19 \pm 0.07$, which have a reduced χ^2 of 0.88 for 267 dof. This energy spectral index of the diffuse emission inside the jet is

consistent with that reported in Hardcastle et al. (2003), viz., $N_H = (1.1 \pm 0.3) \times 10^{21}$ cm^{-2} and $\alpha_X = 1.00^{+0.16}_{-0.15}$, derived for the extended jet emission in the jet between knot A2 and the knot B region (approximately $20'' \leq r \leq 70''$), excluding all compact X-ray features. Interestingly, in the 100 kpc long jet in the radio galaxy Pictor A, the observed X-ray spectral index is constant along the jet, and is $\alpha_X \sim 1$ (Wilson et al. 2001), as in the kiloparsec-scale jet analyzed here, suggesting the action of similar particle acceleration processes for the high-energy electrons resulting in the synchrotron X-ray emission.

3.2. *Transverse Jet Profiles*

We next integrate the photon counts in each narrow sector with an angular width $\Delta\Theta$ over certain radial distances (selected in the range $50'' \leq r \leq 250''$), and then construct the transverse intensity profiles in $\Delta\Theta = 1°$ steps, from $\Theta = 20° - 50°$. We do not examine the innermost part of the jet ($r \leq 50''$) because of the strong absorption due to the dust lane, as discussed in the previous section. Moreover, we cannot determine the position angle Θ in the inner jet region with sufficient accuracy. For example, the $\sim 1''$ diameter of a typical *Chandra* image resolution corresponds to $\Delta\Theta \geq 1°$ at $r \leq 50''$, which is larger than the angular step size of $\Delta\Theta = 1°$ for our analysis. Note that α at $r = 250''$ corresponds to $\approx 4.''4$, or to a linear scale of ≈ 70 pc. Figure 5 shows the transverse jet profiles thus produced for both soft X-rays (0.4–1.5 keV; *top*) and hard X-rays (1.5–8.0 keV; *bottom*). We made separate plots of the transverse profiles for $r \leq 170''$ and $r \geq 170''$, because the jet's emission decreases to the background level at $170''$, but then gradually increases again to a peak at $r \sim 210''$ (see Figs. 1 and 2). The dotted histograms show the profiles derived from the raw X-ray images, whereas those for the diffuse X-ray emission are given as the data points on the solid-line histogram. The transverse jet profile of the diffuse emission shows a flat-top structure for the jet region between $50''$ and $170''$, but, in contrast, a single, narrow peak for the outermost part of the jet ($170'' \leq r \leq 250''$). Such an edge-brightened structure, as observed for the inner jet region, is not readily apparent in the asymmetric intensity profile derived from the raw data.

The flat-topped intensity profile along the transverse jet direction in Cen A cannot be explained by a homogeneous plasma
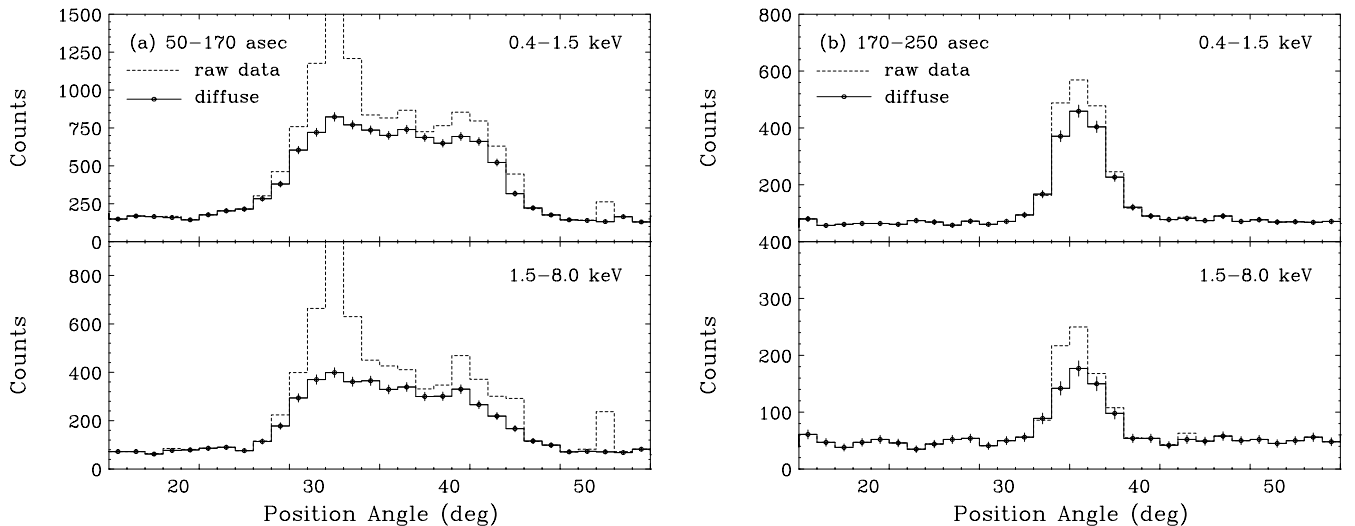

FIG. 5.—Transverse jet profile of the Cen A in the soft X-ray energy band (0.4–1.5 keV) and the hard X-ray energy band (1.5–8.0 keV). The profiles for (*a*) the inner jet region ($50'' \leq r \leq 170''$) and (*b*) the outer jet regions ($170'' \leq r \leq 250''$) are given in separate panels. The dashed histogram shows the profile derived from the raw X-ray image (Fig. 1, *left*), whereas the solid histogram with the data points shows that obtained for the diffuse emission only (Fig. 1, *right*).

fluid moving with a uniform velocity. One natural and simple possibility to account for the observed profile is to consider a stratified model for the kiloparsec-scale Cen A jet, with a velocity shear across the jet outflow. In general, such a structure is actually required to explain many observed properties of extragalactic jets, and is also expected on the grounds of theoretical and numerical jet studies (see the discussion in Stawarz & Ostrowski 2002 and references therein). In this model, different Doppler enhancements of the emission produced within different velocity components can result in the observed limb-brightening of the jet. The other possibility discussed in the literature is to consider a mildly relativistic jet bulk velocity and the enhanced emissivity of the nonthermal plasma at the jet boundaries resulting from, e.g., non-uniform radial structure of the jet magnetic field due to jet interaction with surrounding medium or some particular large-scale magnetic topology (see, e.g., the discussion in Owen et al. 1989). Because of the apparent one-sidedness of the kiloparsec-scale jet in Cen A, we favor the former possibility as the dominant factor shaping the transverse intensity profile, although both Doppler favoritism and plasma emissivity stratification may both play a role.

The exact velocity profile across the kiloparsec-scale jet in Cen A cannot be precisely modeled with the present data. Let us, however, underline a few appropriate constraints. First, note that the observed parallel magnetic field structure along the jet axis, with no evidence for the transverse component that is usually observed in FR I sources, is consistent with a well-developed velocity shear (see in this context Laing & Bridle 2002). Second, if the limb-brightening of the diffuse X-ray emission is predominantly due to varying Doppler enhancements of different jet axisymmetric layers, and the emissivity is *uniform* along the jet (although this may not be a realistic assumption for a stratified jet), a component for which the emission is most strongly beamed toward the observer is the one characterized by the bulk velocity $\beta(\Theta) = \cos \alpha$ [or bulk Lorentz factor $\Gamma(\Theta) = 1/\sin \alpha$], where α is the jet viewing angle. With the preferred $\alpha \sim 50^\circ$ (Tingay et al. 1998; Kraft et al. 2003), one can roughly estimate the bulk velocity of the limb-brightened regions ($\Theta \sim 30^\circ$ and $\sim 40^\circ$) as $\beta \sim 0.65$ (or $\Gamma \sim 1.3$). This very rough, illustrative estimate indicates that the spine of the kiloparsec-scale jet in Cen A—at the position angle $\Theta = 35^\circ$—is most likely still relativistic, with a bulk Lorentz factor $\Gamma \geq 2$. In this context, the single narrow peak at the outermost part of the jet ($170'' \leq r \leq 250''$) may correspond to the spine, decelerated significantly at the terminal part of the collimated outflow. Finally, we note that the half-opening angle of the X-ray jet, $\phi_X \leq 5^\circ$, is smaller than that of the radio jet structure $\phi_R \sim 10^\circ$ for $r > 60''$ (Clarke et al. 1992; see also Kraft et al. 2002). In the framework of the above discussion, this would be consistent with the boundary shear layer spreading in the transverse direction as the jet propagates.

Similar to the analysis in the longitudinal direction, we divided the 1.5–8.0 keV transverse jet profile by that of the 0.4–1.5 keV, to examine the hardness ratio (HR) variation across the X-ray jet. Figure 6 compares the HR and the 0.4–8.0 keV X-ray intensity profiles. Here we divided the inner jet region further into three separate sectors, $50'' \leq r \leq 80''$ (Fig. 6a), $80'' \leq r \leq 120''$ Fig. 6b), and $120'' \leq r \leq 170''$ (Fig. 6c), for a detailed comparison of changes in transverse profile. Edge-brightened structure is most clearly seen in the profile derived for $50'' \leq r \leq 80''$ (Fig. 6a). Interestingly, one can clearly see that the HR is almost uniform across the jet, but shows a weak sign of enhancement at the very edges of the X-ray jet regions ($\Theta \sim 25^\circ$ and $\Theta \sim 45^\circ$), followed by a sudden "drop" (softening) close to the edges. Similar hardening or softening may explain some

variation of the HR even for the jet edges in Figures 6b and 6c. We may speculate that the spectrum changes considerably at the outer edges of the jet, accounting for these variations, although the present data do not allow this to be established.

First, since the HR contains a significant contribution from background photons, apparent changes in HR might be due to variation in the background characteristics rather than changes in the source spectrum itself. This effect is important especially at the jet edges, where the emission is dominated by background photons. We carefully examine this problem later by choosing an appropriate background for spectral fitting. Second, it is well known that the response of the *Chandra* X-ray mirror changes with the incident X-ray energy. The half-power diameter of the PSF is $0''.5$ at 1 keV, but slightly worse at higher energies (e.g., $1''$ at 5 keV; see footnote 6). Such an energy dependence of the angular resolution might introduce HR variations perpendicular to the Cen A jet, especially at the jet edges. To check for this effect quantitatively, we smoothed the 0.4–8.0 keV image (Fig. 1, *right*) with Gaussian functions of $\sigma = 0''.5$ and $1''.0$ to mimic the images obtained in different energy bands. The resultant intensity profiles have only negligible (less than 2%) changes in the HR across the jet, suggesting that we cannot explain the observed hard X-ray features shown in Figure 6 by this effect alone.

Finally, variations of HR may be caused by any possible artifact caused by `dmfilth` and inclusion of background. We therefore remove all the point sources detected by `wavdetect` and fit the diffuse emission with a power-law function in XSPEC, without filling the "holes" remaining after subtracting the source ellipses. We assume a fixed absorption column density of $N_H = 0.96 \times 10^{21}$ cm^{-2}, which is valid all along the jet if $r \geq 50''$ (see § 3.1). We take the background from two sectors just outside the jet ($19^\circ \leq \Theta \leq 23^\circ$ and $47^\circ \leq \Theta \leq 51^\circ$ within an equal $r \sim r + \Delta r$) and subtract them from the source spectrum. The result of spectral fitting across the jet with $\Delta \Theta = 2^\circ$ steps is shown in Figure 7. Although the photon counts are inevitably poor at the jet edges, the general trends of the flux variations and spectral changes are very similar to those expected from the HR profiles. The spectral index seems to increase slightly and gradually along the main jet, being $\alpha_X \geq 1.0$. In addition, the hardest X-ray spectra are observed at the edges of the jet in the $50'' \leq r \leq 80''$ region, where $\alpha_X = 0.23^{+0.93}_{-0.71}$ for $\Theta \sim 25^\circ$ or $\alpha_X = 0.40^{+0.64}_{-0.58}$ for $\Theta \sim 45^\circ$. We note that the background spectrum is approximately represented by a power-law with an energy spectral index of $\alpha_X \sim 1.5 - 2.0$, and therefore background contamination cannot produce an X-ray spectrum as hard as that observed in Figure 7a. Unfortunately, the photon statistics are insufficient to confirm that the X-ray spectrum is actually harder at the very edges of the jet. Nevertheless, this provides an important motivation for future deep observations of the Cen A jet.

3.3. *Diffuse or Unresolved?*

As pointed out by Kraft et al. (2002), the X-ray morphology of the Cen A jet is much more complex when observed at higher spatial resolution. This raises the question whether some fraction of the extended emission discussed in this paper can be explained by the pile-up of small-scale knots below the resolution limit for *Chandra* point-source detection. To estimate what part of the remaining unresolved emission of the jet could indeed result from a large number of unresolved low-luminosity compact features, we construct a luminosity function (LF) for the already resolved jet knots, presented in Figure 8. Here we consider the 32 jet knots located between $50''$ and $250''$ as the strong absorption due to the dust lane makes determination of the unabsorbed luminosity quite uncertain for $r \leq 50''$. We assume a power-law
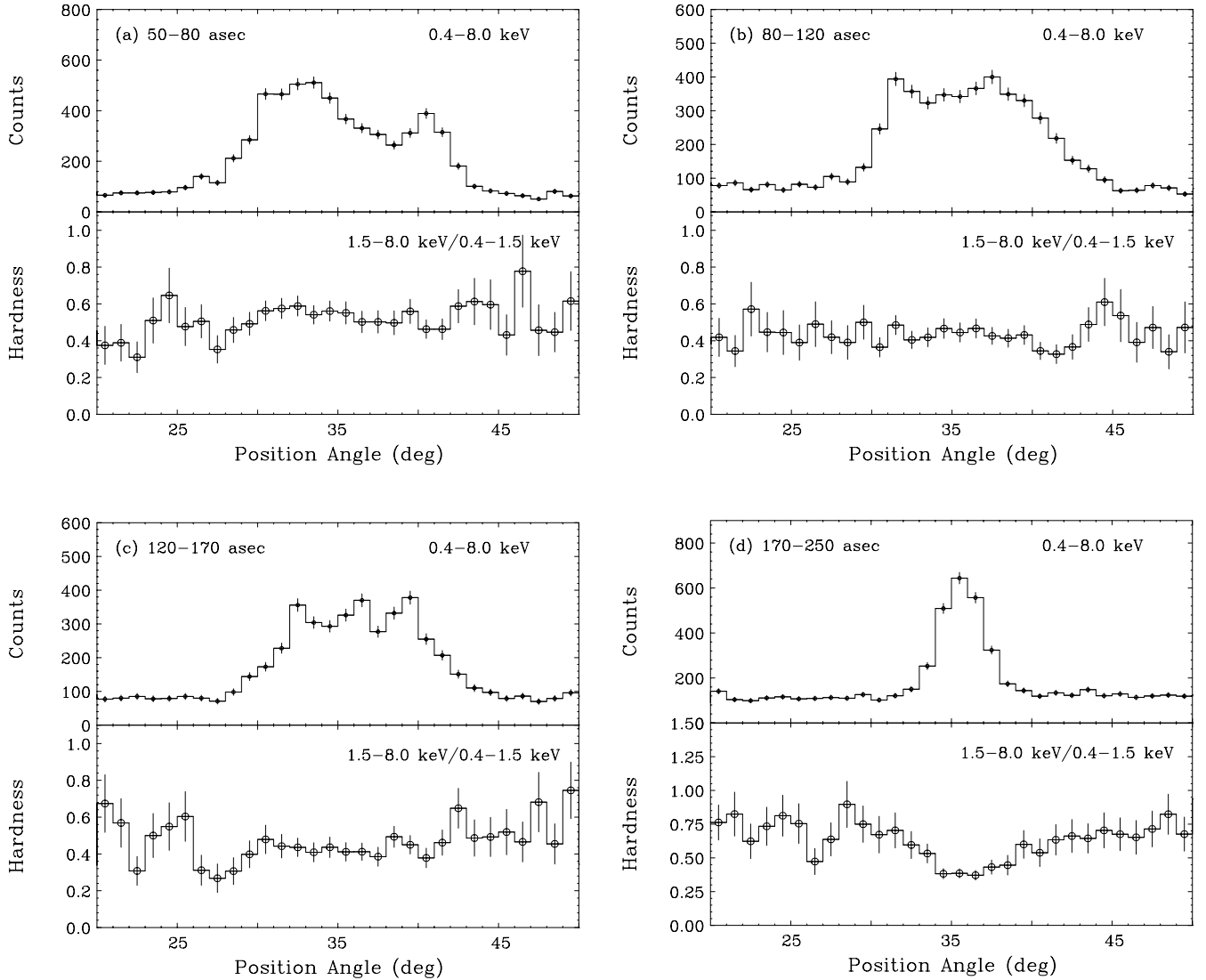
Fig. 6.—*Top panels:* The observed transverse X-ray intensity profile of the diffuse jet component in the 0.4–8.0 keV photon energy band. *Bottom panels:* Variation of the hardness ratio in the direction perpendicular to the jet main axis. Hardness is defined as the ratio between the X-ray counts measured in the soft X-ray energy band (0.4–1.5 keV) and the hard X-ray energy band (1.5–8.0 keV). The profiles are given in separate panels for various distances from the nucleus, (*a*) $50'' \leq r \leq 80''$, (*b*) $80'' \leq r \leq 120''$, (*c*) $120'' \leq r \leq 170''$, and (*d*) $170'' \leq r \leq 250''$. Note the possible hardness variations near the edges of the jet, $\Theta \sim 25°$ and $\Theta \sim 45°$.

energy spectrum with the spectral index $\alpha_X = 1.0$ (Hardcastle et al. 2003; Kraft et al. 2002) and $N_H = 0.96 \times 10^{21}$ cm^{-2} (see § 3.1) to estimate the 0.5–5 keV luminosities of the knots. Although Kraft et al. (2002) derived their LF for 0.1–10 keV luminosities of the knots with a different choice of spectral parameters ($\Gamma_X = 2.3$ and $N_H = 1.7 \times 10^{21}$ cm^{-2}), a rough conversion to their 0.1–10 keV fluxes can be obtained by multiplying our 0.5–5 keV luminosities by a factor of 3.

The limiting sensitivity for this analysis is somewhat uncertain due to source confusion and possible variations of spatial extent among the jet knots. Furthermore, the sensitivity of the observation varies across the field of view due to the telescope vignetting and variations in the PSF. A detailed computation of the limiting sensitivity requires a Monte Carlo simulation taking into account the unknown morphology of the *intrinsic* diffuse emission and is beyond the scope of this paper. Here we follow the simplified method adopted by Kraft et al. (2001): we use the measured background and the telescope PSF at the edge of the field of view and we require a 4 σ measurement of the count rate. Our conservative estimate (using the background map and the

telescope vignetting; Kraft et al. 2001) provides a sensitivity limit of $L_{sens} \sim 4 \times 10^{36}$ ergs s^{-1}. Let us briefly discuss this value. During these observations the encircled energy of a point source is contained within a diameter of $\sim 3''$ all along the jet. Assuming that the intrinsic spatial extent of the knots is less than $4''$, we conservatively expect that all the compact sources can be detected within a circle of $\sim 6''$ diameter, even if they are in the outermost part of the jet (i.e., $\geq 4'$ off axis with respect to the mirror focus). The typical background within this region is ~ 15 counts from the observational data. To detect a knot at the required statistical level, we therefore need ~ 25 net source counts excluding the background photons. This corresponds to an X-ray luminosity of $L_{sens} = 2 \times 10^{36}$ ergs s^{-1}. If a similar knot is embedded in extended emission (as observed in $50'' \leq r \leq 80''$), ~ 50 net photons are required over the ~ 120 background photons. It is therefore reasonable to assume $L_{sens} = 4 \times 10^{36}$ ergs s^{-1} in the following discussion.

In Figure 8 the hatched region shows where our sampling is incomplete and somewhat biased. The overall LF is well modeled by a broken power law, with the power-law slope flatter
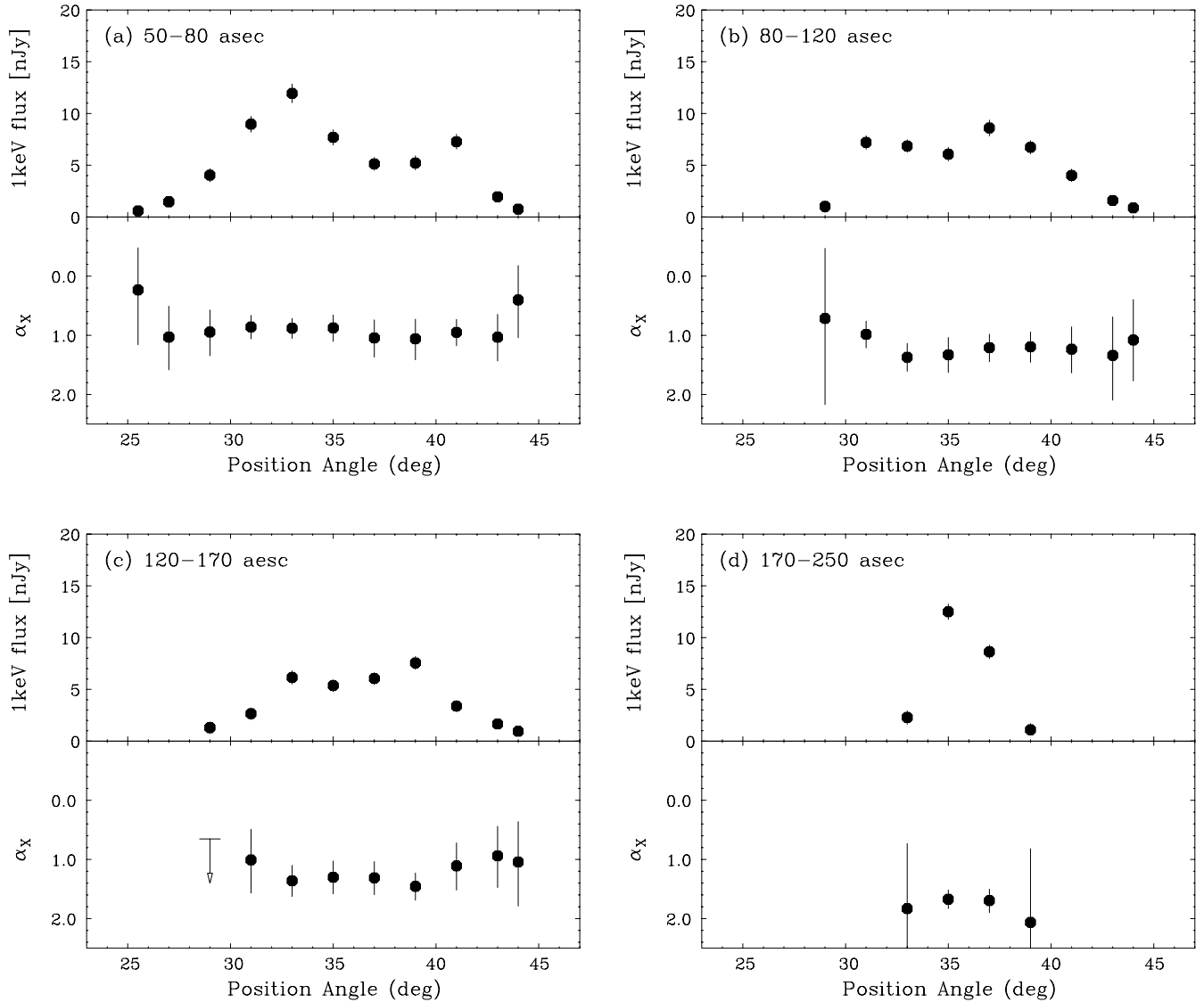
Fig. 7.—Variation of the X-ray intensity measured at 1 keV (*top panels*), and the energy spectral index (*bottom panels*) across the jet, in $\Delta\Theta = 2°$ steps. The contribution of point sources is simply removed, and `dmfilth` is not used in order to avoid any possible artifacts in the spectral analysis. Reduction of integration regions due to the point-source subtraction is corrected in estimating the 1 keV flux. The fitting model consists of a power-law function and the assumed Galactic absorption column density $N_H = 0.96 \times 10^{21}$ cm^{-2}.

below the break. The dashed line on Figure 8 shows the fit considered hereafter, where the power-law slope [κ of $N(>L_X) \propto L_X^{-\kappa}$] flattens significantly from $\kappa = 1.4$ to 0.5 below $L_{brk} \simeq 9 \times 10^{36}$ ergs s^{-1}. The maximum likelihood method of Crawford et al. (1970), using separate data sets below and above the break, supports this fit with an uncertainty (defined here as a standard deviation) of $\sigma \simeq 0.4$ for each κ. However, due to the limited number of the detected jet knots (24 for $L_X \geq 4 \times 10^{36}$ ergs s^{-1}), the Kolmogorov-Smirnov test (Press et al. 1992) indicates that a single power-law model with $\kappa \sim 0.7$ is also statistically acceptable. Even so, a single steep power law with $\kappa \geq 1.0$ can be rejected at the >90% confidence level. Assuming further that the distribution of knot luminosities extends down to some minimum value L_{min}, the integrated total X-ray luminosity can be evaluated quantitatively for both the resolved and the unresolved jet knots (see Kraft et al. 2002 for the detailed formalism). We note that the total luminosity of the Cen A jet (i.e., the sum of the jet knots and the unresolved diffuse emission) is 1.6×10^{39} ergs s^{-1}. Meanwhile, by integrating the LF down to any value of L_{min} we get $<8.1 \times 10^{38}$ ergs s^{-1}, at most, if we assume the "best-fit" broken

power-law LF described above. Note that this is only 25% larger than the sum of the *already resolved* jet knots. The situation is almost unchanged if we take a single power-law function with $\kappa \simeq 0.7$ for the LF. We therefore conclude that about half of the total jet emission, $L_X \sim 8 \times 10^{38}$ ergs s^{-1}, is truly diffuse in nature.

We finally consider an apparent discrepancy between our results and previous reports. Kraft et al. (2002) suggested that the diffuse X-ray emission of the Cen A jet may be entirely explained by unresolved knots only if $L_{min} = 3 \times 10^{35}$ ergs s^{-1} and there is no break in the LF below the sensitivity limit of $L_{sens} \sim 3 \times 10^{37}$ ergs s^{-1} (corresponding to $L_X \sim 1 \times 10^{37}$ ergs s^{-1} in our LF). There are several possibilities to account for this discrepancy. First, the sensitivity limit adopted in Kraft et al. (2002) is calculated for a single $\sim$35 ks observation. As discussed in detailed in Kraft et al. (2001), the sensitivity is limited by the source luminosity, not by the background, over the most of the field of view. Therefore, our analysis based on the co-added ACIS-S image (95 ks exposure in total) provides a factor of $\sim\sqrt{3}$ deeper sensitivity for the source detection. Moreover, the PSF in the
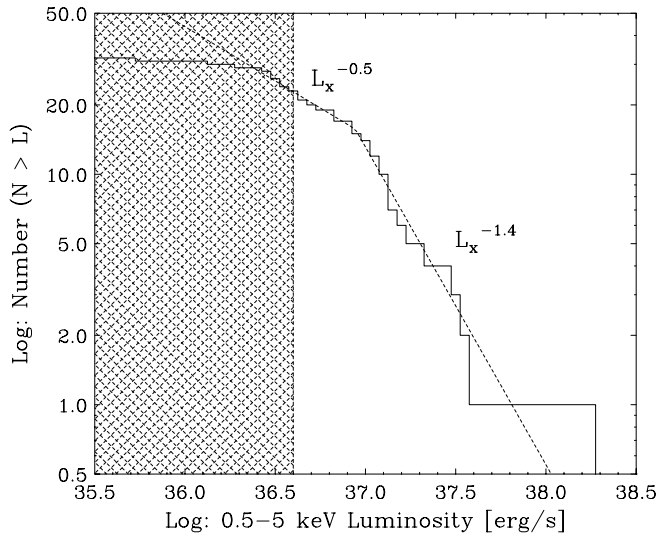
Fig. 8.—Luminosity function of the knots in the jet, constructed excluding the knots of the innermost part of the outflow ($0'' \leq r \leq 50''$). The X-ray luminosity is the absorption corrected luminosity in the 0.5–5.0 keV band, assuming a power-law spectrum with energy spectral index $\alpha_X = 1.0$ and $N_H = 0.96 \times 10^{21}$ cm^{-2}. The best-fit broken power-law model, excluding the cross-hatched region where our sample is incomplete and biased ($L_X \leq 4 \times 10^{36}$ ergs s^{-1}), is also shown.

inner jet is a factor of ~ 2 smaller than previous observations (see § 2), which further improves the signal-to-noise ratio. Second, by applying the same sensitivity limit as Kraft et al. (2002), it would be difficult to see a flattening in the low-luminosity part of the LF. Thus, a steep power-law LF is consistent with the work of Kraft et al. (2002; who obtained $\kappa = 1.1$), although is implausible when the low-luminosity range ($L_X < 10^{37}$ ergs s^{-1}) is taken into account. Third, it seems that quite different conclusions can be reached for different choices of κ. In fact, integration of the LF down to arbitrarily small $L_{\min}$ approaches infinity if $\kappa \geq 1$. Future deep observations of the Cen A jet are therefore strongly encouraged, although it seems to us reasonable that a significant fraction of the X-ray jet emission in this source is actually diffuse.

4. DISCUSSION

4.1. The Jet

The observed X-ray spectral index of the diffuse emission within the whole jet—including both the central flow and the limb-brightened edges—is steep, $\alpha_X \simeq 1.0-1.2$. The implied energy distribution of the X-ray synchrotron emitting electrons therefore has to be $n_e(\gamma) \propto \gamma^{-s}$ with $s = 2\alpha_X + 1 = 3.0-3.4$, where γ is the electron Lorentz factor. Such a spectrum is very similar to the one observed in the compact knots, which are believed to be the sites of shock waves, suggesting that the same, or a similar, particle acceleration process is acting in both regions. In the case of the shock acceleration, however, one expects the energy spectral index of the freshly accelerated electrons to be $s_{in} = 2.0$ in the strong nonrelativistic regime, or $s_{in} \gtrsim 2.0$ when relativistic plasma velocities are considered (see, e.g., Kirk & Duffy 1999; Ostrowski 2002). Thus, if first-order Fermi shock acceleration is indeed responsible for formation of the X-ray (synchrotron) emitting electrons within the Cen A jet, the observed particle energy spectrum—both within and outside the resolved knots—has to be already modified by the (dominant) synchrotron losses, i.e., the spectral index of freshly accelerated high-energy electrons has to be increased by the radiative cool-

ing $|\dot{\gamma}|_{\rm syn} = \sigma_T \gamma^2 B^2 / 6\pi m_e c$ to $s = s_{in} + 1$ (the "strong cooling regime" with homogeneous magnetic field B; see Kardashev 1962). In fact, the appropriate cooling timescale is very short, $t_{\rm syn} = \gamma / |\dot{\gamma}|_{\rm syn} \sim 20\ B_{-4}^{-3/2}\varepsilon_{10}^{-1/2}$ yr (for a jet magnetic field $B_{-4} \equiv B/10^{-4}{\rm G} \sim 1$, an observed synchrotron photon energy $\varepsilon_{10} \equiv \varepsilon/10$ keV ~ 1, and a jet Doppler factor $\delta \sim 1$), consistent with this interpretation. We note in this context that the detailed analysis of the radio emission from a number of FR I sources of Young et al. (2005) revealed a "universal" injection spectral index for the radiating electrons of $s_{in} = 2.1$, in accordance with the above discussion. We also note that synchrotron cooling within a non-uniform magnetic field can result in a spectral break larger than the standard one discussed above, $s > s_{in} + 1$ (e.g., Bicknell & Begelman 1996).

On the other hand, the very short synchrotron lifetime and the extended character of the diffuse X-ray jet component discussed here indicate that the appropriate acceleration process for the X-ray–emitting electrons cannot be connected exclusively with the localized compact knots of the kiloparsec-scale jet, but instead has to operate effectively throughout the whole jet volume. Indeed, the maximum propagation length of the jet electrons emitting 10 keV synchrotron photons within the 100 μG jet (equipartition) magnetic field can be estimated as $l_{\rm rad} = c\Gamma t_{\rm rad} \sim 10$ pc for $\Gamma \sim 2$, which clearly indicates the need for the continuous acceleration of the radiating electrons in between the compact knots. Let us mention at this point, that the analysis of the expected γ-ray emission from kiloparsec-scale FR I jets presented by Stawarz et al. (2006) suggests that subequipartition magnetic fields (which could increase $l_{\rm rad}$) are not likely in these objects. The problem could disappear if many small-scale *strong* shocks are present (below the flux resolution limit for our point-source detection), possibly generated at the supersonic and highly turbulent jet boundary layer. However, as argued in the previous section, based on the constructed luminosity function for the resolved jet knots, the observed extended X-ray emission is most likely truly diffuse in nature, and not just the pile-up of the unresolved compact knots.

A physical process that can naturally account for the distributed continuous acceleration of the radiating electrons within the whole jet volume consists of interaction of the particles with turbulent MHD waves. Indeed, by applying quasi-linear theory for particle-wave interactions (see, e.g., Schlickeiser 1989), one can find that with a reasonable set of physical parameters for the Cen A jet, the available maximum energies of the electrons accelerated in this way may be high enough to alow for efficient production of the synchrotron X-rays. On the other hand, the resulting electron energy spectrum is expected to be very flat: with a one-dimensional power spectrum of Alfvénic turbulnce $W(k) \propto k^{-q}$ and a "typical" range of turbulence spectral index $q \in (1, 2)$—usually obtained in phenomenological models for the astrophysical MHD turbulence (see, e.g., the recent review by Muller & Biskamp 2003, and references therein)—the steady-state solution for the momentum diffusion equation is a power law with $s_{in} = q - 1$ between 0 and 1 (see, e.g., Borovsky & Eilek 1986 or Park & Petrosian 1995). However, the observed X-ray spectral index of the diffuse component of the Cen A jet is steep, requiring an electron energy slope of $s \simeq 3$. In particular, taking the expected injection spectrum with s_{in} either 0 or 1, the strong (synchrotron) cooling regime condition gives an observed electron energy index of $s = 2$ in both cases (see Aharonian 2002), or an expected X-ray power-law slope $\alpha_X = 0.5$, i.e., much flatter than observed. It is important to note, however, that the quasi-linear theory for particle-wave interactions is of limited applicability for physical conditions within extragalactic jets,

which may be highly turbulent, even with a possibly dynamically important pressure due to ultrarelativistic particles at the jet boundary (see Ostrowski 2000). In particular, the expected large ratio of the escape to the radiative losses timescales within the jet (see Stawarz & Ostrowski 2002) means that the stationary solution may not be realizable due to accelerated particle back-reaction, or that the turbulent diffusion could dominate the escape process. In such cases the quasi-linear approach may no longer be valid. In addition, radiative effects within a nonuniform magnetic field can modify the high-energy part of the electron energy distribution in a nontrivial way. A set of such problems is under investigation.

4.2. Hard Outer Sheath?

Our analysis indicates the possible presence of hard X-ray features within the outer (fragmentary) sheath of the Cen A kiloparsec-scale jet, extending beyond the X-ray limb-brightened jet edges. The X-ray spectral properties of the outer jet boundaries are most probably very different from the ones characterizing the central jet flow. In particular, the observed X-ray spectral index can be as flat as $\alpha_X < 0.5$. In addition, the physical connection of these regions to the main flow is not clear, although they do roughly coincide with the edges of the radio structure. One may note in this context that detailed studies of the extragalactic radio jets using the "spectral tomography" technique has also revealed the presence of some features along the outer jet boundaries. In particular, Katz-Stone & Rudnick (1997) showed that the large-scale jet in the FR I radio galaxy 3C 449, for which the radio spectral index $\alpha_R \approx 0.5$ is roughly constant along the whole jet, is surrounded by a steep-spectrum radio "sheath." Also, large-scale jets in the FR II radio galaxy Cygnus A are placed in the edge-brightened "channels," which are consistent with the enhancement of radio-emitting electrons at the outer jet boundaries (Katz-Stone & Rudnick 1994).

Unfortunately, the present X-ray data are not sufficient to convincingly demonstrate the presence of a hard sheath around the Cen A jet. Let us, however, mention briefly a possible scenario that can account for formation of such hard features, namely, synchrotron emission of the high-energy electrons that lose energy predominantly due to inverse Compton radiation in the Klein-Nishina regime (hereafter the "IC/KN" process; see Aharonian & Ambartsumyan 1985; Dermer & Atoyan 2002; Kusunose & Takahara 2005; Khangulian et al. 2005; Moderski et al. 2005). An interesting aspect of this scenario is that the observed electron spectrum can be flatter than the injected one, with the asymptotic power-law slope $s \approx s_{in} - 1$. Let us therefore assume that the acceleration process similar to the one operating within the jet acts also within the outer boundaries of the outflow, where the magnetic field intensity is possibly lower than within the jet. Thereby the high-energy electrons cool partly due to the synchrotron emission, producing X-ray photons, but mostly due to the IC/KN radiation at γ-ray frequencies. The dominant IC/KN process thus flattens the injected electron spectrum, leading to the observed flat X-ray (synchrotron) continuum.

The Lorentz factor of electrons emitting 0.1 keV synchrotron photons is $\gamma_X \approx 10^7 B_{-4}^{-1/2}$. Hence, the required energy of the seed photons to be upscattered by these electrons in the KN regime is $\varepsilon_0 > m_e c^2/4\gamma_X \sim 10^{-2} B_{-4}^{1/2}$ eV. At the same time, the energy density of the seed photons has to be $U_0 > U_B \approx 4 \times 10^{-10} B_{-4}^2$ ergs cm^{-3} in order to ensure the dominance of the IC/KN losses. Taking the lowest expected value $B_{-4} \sim 0.01$, this already excludes the cosmic microwave background radiation as the source of seed photons. However, Cen A is a giant elliptical galaxy known for its strong infrared emission: $S_{IR} = 23$ Jy at $\lambda_{IR} = 12$ μm (Knapp et al. 1990). Assuming that all of this radiation is produced within $r = 1$ kpc from the galactic center (see Israel 1998), one can obtain a rough estimate for the energy density of the galactic ~ 0.1 eV photons at the position of the kiloparsec-scale Cen A jet, $U_{IR} = S_{IR} d_L^2/r^2 \lambda_{IR} \sim 2 \times 10^{-12}$ ergs cm^{-3}, close to the average value for giant ellipticals, $\sim 10^{-11}$ ergs cm^{-3}, found by Stawarz et al. (2003). Note that this is about 2 orders of magnitude lower than the expected energy density of the $\lambda_{star} \sim 1$ μm starlight energy density (Stawarz et al. 2003). Also, the energy density of the synchrotron infrared emission of the nuclear jet in Cen A can be important in this respect. In particular, taking the observed synchrotron luminosity of the Cen A nuclear jet $L_{bl} \approx 3 \times 10^{41}$ ergs s^{-1} and its critical observed synchrotron frequency $\nu_{bl} \approx 10^{12}$ Hz (Chiaberge et al. 2000), one gets the appropriate energy density as measured by a stationary observer located on the jet axis at $r = 1$ kpc from the active center $U_{bl} = L_{bl}\Gamma_{bl}^3/4\pi r^2 c \sim 10^{-10}$ ergs cm^{-3}, and the appropriate critical frequency $\Gamma_{bl}\varepsilon_{bl} \sim 0.03$ eV, for the expected bulk Lorentz factor of the nuclear jet $\Gamma_{bl} \sim 10$ (see Stawarz et al. 2003). Relative enhancement of synchrotron emission produced within a structured relativistic jet may constitute an alternative/additional source of the seed infrared photons (see in this context Ghisellini et al. 2005). Thus, we conclude that if only the magnetic field in the outer sheath of the kiloparsec-scale Cen A jet is $B \approx 10$ μG can the suggested hard X-ray emission result from synchrotron radiation of the high-energy electrons characterized by the standard initial spectrum $s_{in} \simeq 2$, which cool mainly by Comptonization of the nuclear jet emission (and also the starlight photon field) in the KN regime.[10]

5. CONCLUSIONS

We have presented an analysis of the diffuse X-ray emission from the kiloparsec-scale jet in Centaurus A. We found that the extended emission is most likely diffuse in nature rather than being the summation of unresolved compact sources and that it exhibits a relatively flat-topped intensity profile with a steep, uniformly distributed spectral index of $\alpha_X \approx 1$, similar to those observed in the compact knots. We interpret the observed X-ray morphology in terms of a stratified jet model, consisting of a relativistic outflow with an expanding turbulent boundary shear layer. We argue that the observed X-ray spectrum of this diffuse component, consistent with the synchrotron emission produced in the strong cooling regime, requires continuous acceleration of ultrarelativistic electrons within the whole jet volume. We also note that the jet may be (partially) surrounded by an outer sheath with a very hard X-ray spectrum. Both the presence and origin of this feature are unclear: we suggest that it forms in a turbulent region just outside the jet, separating the main outflow from the external medium, where the conditions for the radiative cooling processes are different from the ones characterizing the jet. Although the present data do not allow us to unequivocally demonstrate the presence of the hard outer sheath, or to determine the appropriate particle acceleration mechanism acting within (and possibly outside) the outflow, our analysis indicates that (1) the jet structure is more complex than that visible on the intensity maps alone, and (2) the acceleration and spectral evolution of the radiating particles may be governed by many different processes (including those such as magnetic field reconnection, which we have not discussed), linked to the complex magnetohydrodynamical configuration of the outflow.

---

[10] We note that the very high energy γ-ray flux of the outer sheath implied by this model, $\sim 10^{-15}$ ergs cm^{-2} s^{-1}, is well below the sensitivity limits of current Cerenkov telescopes.

REFERENCES

Aharonian, F. A. 2002, MNRAS, 332, 215
Aharonian, F. A., & Ambartsumyan, A. S. 1985, Astrofizika, 20, 499
Bicknell, G. V., & Begelman, M. C. 1996, ApJ, 467, 597
Borovsky, J. E., & Eilek, J. A. 1986, ApJ, 308, 929
Celotti, A., Ghisellini, G., & Chiaberge, M. 2001, MNRAS, 321, L1
Chiaberge, M., Celotti, A., Capetti, A., & Ghisellini, G. 2000, A&A, 358, 104
Clarke, D. A., Burns, J. O., & Feigelson, E. D. 1986, ApJ, 300, L41
Clarke, D. A., Burns, J. O., & Norman, M. L. 1992, ApJ, 395, 444
Colbert, E. J. M., Heckman, T. M., Ptak, A. F., Strickland, D. K., & Weaver, K. A. 2004, ApJ, 602, 231
Crawford, D. F., Jauncey, D. L., & Murdoch, H. S. 1970, ApJ, 162, 405
Dermer, C. D., & Atoyan, A. M. 2002, ApJ, 568, L81
Ghisellini, G., Tavecchio, F., & Chiaberge, M. 2005, A&A, 432, 401
Hardcastle, M. J., Birkinshaw, M., & Worrall, D. M. 2001, MNRAS, 326, 1499
Hardcastle, M. J., Worrall, D. M., Kraft, R. P., Forman, W. R., Jones, C., & Murray, S. S. 2003, ApJ, 593, 169
Harris, D. E., & Krawczynski, H. 2002, ApJ, 565, 244
Harris, D. E., Mossman, A. E., & Walker, R. C. 2004, ApJ, 615, 161
Hillas, M. 1984, ARA&A, 22, 425
Israel, F. P. 1998, A&A Rev., 8, 237
Kardashev, N. S. 1962, Soviet Astron.–AJ, 6, 317
Kataoka, J., Edwards, P., Georganopoulos, M., Takahara, F., & Wagner, S. 2003a, A&A, 399, 91
Kataoka, J., & Stawarz, Ł. 2005, ApJ, 622, 797
Katz-Stone, D. M., & Rudnick, L. 1994, ApJ, 426, 116
———. 1997, ApJ, 488, 146
Khangulian, D., & Aharonian, F. A. 2005, in AIP Conf. Ser. 745, High Energy Gamma-Ray Astronomy: 2nd International Symposium, ed. F. A. Aharonian, H. J. Völk, & D. Horns (New York: AIP), 359
Kirk, J. G., & Duffy, P. 1999, J. Phys. G, 25, 163
Knapp, G. R., Bies, W. E., & van Gorkom, J. H. 1990, AJ, 99, 476
Kraft, R. P., Forman, W. R., Jones, C., Murray, S. S., Hardcastle, M. J, & Worrall, D. M. 2002, ApJ, 569, 54
Kraft, R. P., Hardcastle, M. J., Worrall, D. M., & Murray, S. S. 2005, ApJ, 622, 149

Kraft, R. P., et al. 2000, ApJ, 531, L9
———. 2001, ApJ, 560, 675
———. 2003, ApJ, 592, 129
Kusunose, M., & Takahara, F. 2005, ApJ, 621, 285
Laing, R. A & Bridle, A. H. 2002, MNRAS, 336, 328
Moderski, R., Sikora, M., Coppi, P. S., & Aharonian, F. A. 2005, MNRAS, 363, 954
Muller, W.-C., & Biskamp, D., in Turbulence and Magnetic Fields in Astrophysics, ed. E. Falgarone & T. Passot (Berlin: Springer), 3
Ostrowski, M. 2000, MNRAS, 312, 579
———. 2002, J. Phys. Stud., 6, 393
Owen, F. N., Hardee, P. E., & Cornwell, T. J. 1989, ApJ, 340, 698
Park, B. T., & Petrosian, V. 1995, ApJ, 446, 699
Press, W. H., Teukolsky, S. A., Vetterling, W. T., & Flannery, B. P. 1992, Numerical Recipes in C (Cambridge: Cambridge Univ. Press)
Rieger, F. M., & Duffy, P. 2004, ApJ, 617, 155
Schlickeiser, R. 1989, ApJ, 336, 243
Schreier, E. J., Burns, J. O., & Feigelson, E. D. 1981, ApJ, 251, 523
Schreier, E. J., Feigelson, E., Delvaille, J., Giacconi, R., Grindlay, J., Schwartz, D. A., & Fabian, A. C. 1979, ApJ, 234, 39
Schwartz, D. A., et al. 2000, ApJ, 540, L69
Stawarz, Ł., Kneiske, T. M., & Kataoka, J. 2006, ApJ, 637, 693
Stawarz, Ł., & Ostrowski, M. 2002, ApJ, 578, 763
Stawarz, Ł., Sikora, M., & Ostrowski, M. 2003, ApJ, 597, 186
Stawarz, Ł., Sikora, M., Ostrowski, M., & Begelman, M. C. 2004, ApJ, 608, 95
Swain, M. R., Bridle, A. H., & Baum, S. A. 1998, ApJ, 507, L29
Tavecchio, F., Maraschi, L., Sambruna, R. M., & Urry, C. M. 2000, ApJ, 544, L23
Tingay, S. J., et al. 1998, AJ, 115, 960
Vikhlinin, A., Forman, W., Jones, C., & Murray, S. 1995, ApJ, 451, 542
Wilson, A. S., Young, A. J., & Shopbell, P. L. 2001, ApJ, 547, 740
Young, A., Rudnick, L., Katz, D., DeLaney, T., Kassim, N. E., & Makishima, K. 2005, ApJ, 626, 748